Applied Geomatics
https://doi.org/10.1007/s12518-022-00482-8

ORIGINAL PAPER

Assessment of the accuracy of low-cost multi-GNSS receivers in monitoring dynamic response of structures

Chenyu Xue[1] · Panos Psimoulis[1] · Alexander Horsfall[1] · Qiuzhao Zhang[2] · Xiaolin Meng[3]

Received: 14 November 2022 / Accepted: 6 December 2022

Abstract

The monitoring of bridges is a crucial operation for their structural health examination and maintenance. GNSS technology is one of the methods which are applied with the main advantage that the direct measurement of the bridge displacement is conducted in an independent global coordinate system. However, the high cost of the GNSS stations, which are consisted of dual-frequency receivers and geodetic GNSS antennas, is the main reason of the limited application of GNSS for bridge monitoring. In this study, we assessed the performance of low-cost multi-GNSS receivers in monitoring dynamic motion, similar to that of bridge response. The performance of the low-cost GNSS receivers was assessed based on controlled experiments of horizontal and vertical motion. For the horizontal motion, controlled experiments of circular motion of various predefined radius between 5 and 50 cm were executed where the low-cost GNSS receivers were assessed against dual-frequency geodetic receivers. For the vertical motion, manually controlled experiments of vertical oscillations of amplitude 8 and 15 mm were executed where the low-cost GNSS receivers were assessed against the Robotic Total Station (RTS). Finally, a low-cost monitoring system formed by two closely spaced low-cost GNSS receivers was applied in dynamic displacement monitoring of the Wilford Suspension Bridge. The analysis of the low-cost GNSS data revealed the beneficial contribution of (i) the multi-constellation on the accuracy and precision of the GNSS solution and (ii) the combination of closely spaced low-cost GNSS receivers, to limit potential cycle slips and the low-cost GNSS noise level and reach accuracy and precision similar to that of geodetic-grade GNSS receivers. This was confirmed in the bridge monitoring application, where the main modal frequency and the response amplitude of the bridge were identified successfully by the low-cost GNSS receivers' data analysis.

Keywords Low-cost GNSS receiver · Multi-GNSS · Structure monitoring · Accuracy · CME filter · Modal frequency

Introduction

Conventional structural health monitoring (SHM) associated with GNSS technology is usually accomplished by high-end survey-grade dual-frequency receivers and geodetic antennas (Meng et al. 2018), which is the major contribution to the high deployment cost associated with GNSS deformation monitoring. This problem aggravates further especially when multiple locations of interest need to be monitored, demanding employment of a large network of sensors. Therefore, the deployment cost is a concerning problem for SHM and eventually constrains its broader applications. However, the recent emergence of certain types of the low-cost GNSS receivers might provide an alternative cost-effective approach (Cina and Piras 2015; Xue et al. 2021).

The survey-grade dual-frequency GNSS receivers are usually priced 10–20 times more than the cheap mass-market GNSS receivers, with the latter having properties such

✉ Panos Psimoulis
Panagiotis.Psimoulis@nottingham.ac.uk

Chenyu Xue
evxcx1@nottingham.ac.uk

Alexander Horsfall
alex.horsfall@ntlworld.com

Xiaolin Meng
mengxl@njut.edu.cn

[1] Nottingham Geospatial Institute, University of Nottingham, Nottingham, UK

[2] School of Environment Science and Spatial Informatics, China University of Mining Technology, Xuzhou, China

[3] Beijing University of Technology, Beijing, China

Published online: 22 December 2022

as light weight, compact, smaller in size, and disposable (Matias et al. 2015). Furthermore, the advancements of modern low-cost receivers also include features such as high-sampling rate and multi-GNSS capacity (Xue et al. 2021). These features indicate the potential for the low-cost GNSS receivers in high-precision applications with reduced budget and make it quite favourable to establish a dense monitoring network.

However, the trade-off is that the current low-cost receivers are mostly single frequency, indicating that the integer ambiguity resolution to reach a 'fixed' solution could be longer compared to dual-frequency receivers especially in the initial observation phase or after false ambiguity fix, mostly known as cycle slip. Takasu and Yasuda (2008) found that the time to first fix (TTFF) was significantly longer for low-cost receivers than geodetic receivers. Apart from that, the ionospheric-free linear combination (LC) is also not possible for single-frequency receivers, and the functionality of the receivers, such as the low-noise amplifier (LNA), front-end receiver hardware multipath mitigation, oscillators, and receiver hardware qualities, is compromised. The low-cost patch antenna also has less gain and suppressed multipath rejection performance compared to geodetic grade antennas (Peppa et al. 2018).

Although comparatively poor signal-to-noise ratio (SNR) GNSS observations are expected from low-cost instrument, empirical research has suggested some low-cost receivers to have the functionality matching with single-frequency geodetic receivers. The positioning accuracy and its RTK capability of low-cost receivers were evaluated by Takasu and Yasuda (2009), and some of the conclusions were that the performance of the single-frequency low-cost receiver could be comparable with that of a single-frequency geodetic receiver. Similar conclusions were also made by Cina and Piras (2015) stating that a similar performance between mass market and geodetic receiver can be achieved under certain conditions such as long acquisition time, short baseline length, and use of external antenna.

Based on previous studies, it has been shown that in a short-baseline network, the grade of rover antenna is important for the solution precision, as when geodetic antenna is used with a low-cost receiver, the solution is more precise than when a patch antenna is used (Zhang and Schwieger 2016). However, for the reference stations, the receiver grade has negligible impact on baseline solutions, whereas better antenna grade would result in better precision (Xue et al. 2021).

Despite the surging research interest into the low-cost GNSS sensors, only few studies have tested their applications in practical deformation monitoring applications. Jo et al. (2013) analysed the feasibility of displacement monitoring using low-cost GPS receiver. Other studies mostly focused on geohazard monitoring such as landslide monitoring (Biagi et al. 2016; Cina and Piras 2015; Heunecke et al. 2011). Also, few studies tested the low-cost GNSS receivers in civil engineering-related SHM applications requiring continuous monitoring apart from Manzini et al. (2022), Poluzzi et al. (2019), and Xue et al. (2022). Therefore, we conducted an experimental study to assess the performance of the low-cost GNSS receivers in monitoring the dynamic horizontal and vertical motion of different amplitudes and frequencies against the performance of geodetic-grade GNSS receivers or the Robotic Total Station (RTS). The performance of the low-cost GNSS receivers was assessed (i) for GPS-only and multi-GNSS solutions, to evaluate the potential contribution of additional GNSS systems on GPS, and (ii) by combining two closely spaced low-cost GNSS receivers, to model the site-specific common errors of the two GNSS receivers (e.g., multipath) and improve the performance of the low-cost GNSS receivers in monitoring dynamic motion. Finally, the performance of the low-cost GNSS receivers was also examined in a bridge deformation monitoring application to conclude whether the bridge response characteristics can be determined accurately.

Experiments: horizontal motion

Experiment design

The aim of the circular horizontal controlled experiments was to assess the performance of the low-cost GNSS measurements in determining the amplitude and frequency of dynamic motion scenarios (i.e., different motion amplitude) against that of dual-frequency geodetic GNSS receivers. The experiments were conducted on the roof of the Nottingham Geospatial Institute (NGI), where the GNSS base station was set up on a control point and the rover receivers/antennas were mounted on the rotation device creating a short baseline of approximately 20 m (Fig. 1). A geodetic GNSS receiver and geodetic antenna were used for the base station, since it has been proved in previous studies the benefit of adopting a geodetic antenna in the base station configuration for the low-cost GNSS receivers' short baseline performance (Xue et al. 2021). Two symmetrical blades were appended on the rotation motor. Driven by the motor, a circular planar motion of constant speed (angular velocity 2.275 rad/s), corresponding to the constant frequency of 0.362 Hz, was executed. Two low-cost u-blox M8T EVK GNSS receivers were used with two patch antennas being deployed on the same side of the blade, closely-spaced and orientated with the same azimuth. On the other side, a Leica GNSS GS10 receiver connected to a Leica AS10 antenna was deployed as the geodetic-grade GNSS rover. The low-cost rovers and geodetic GNSS rover were setup so that they co-rotate with same rotation radius with respect the rotation centre. There were executed experiments of different rotation radii ranging

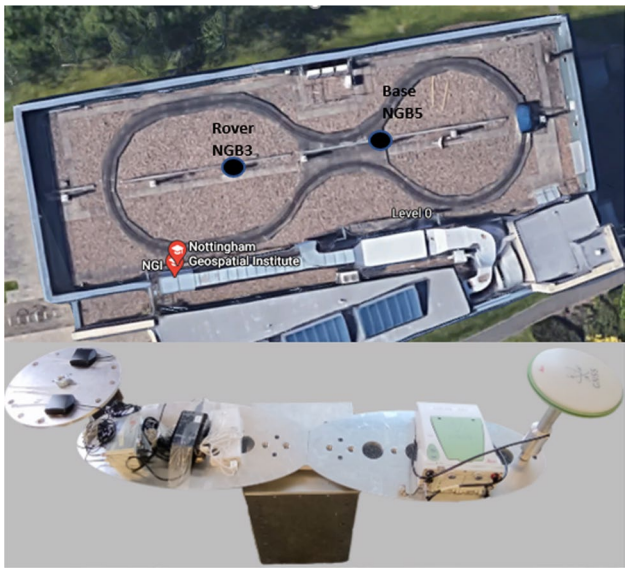

Fig. 1 Top panel: the plan view of the experiment site (in courtesy of Google map): where the rover was placed at NGB3 and the base located at NGB5. Bottom panel: the layout of the GNSS rovers on the rotation device which was placed at NGB3 (two u-blox rovers on one side and one geodetic rover on the other side)

between 5 and 50 cm. Both u-blox and Leica receivers were configured to record GPS, GLONASS, and Galileo constellation observations with 10 Hz sampling rate.

GNSS data processing and analysis

The GNSS data of the base and rover stations were processed using the double difference process mode and the open-source software RTKLIB 2.4.3 (demo5 b33c). The RTKLIB 2.4.3 (demo5 b33c) is an improved and modified version of RTKLIB 2.4.3, which was developed by Everett (2020), with the main improvement to be the additional constraints for ambiguity resolution to reduce false fixes. Further details of the RTKLIB version used in this study can be found in Everett (2016). The GNSS solutions led to coordinate time series of the GNSS rovers in *Northing (N)*, *Easting (E)*, *and Up (U)* components with respect to the GNSS base station. Then, the time series of the low-cost GNSS receivers were compared against the Leica receiver time series, in terms of the precision of the *E/N/U* coordinates and the *R* (radius) of the circular motion executed in each experiment.

Assuming that the rotating device was executing a precise circular trajectory, a model was fitted using the actual measurements of the GNSS time series. The comparison between the circle characteristics (radius and frequency) is defined by the GNSS measurements against the real circle characteristics defined by the accuracy of the measurements, while the residuals of the GNSS time series are defined by the precision of the measurements. To calculate the circle radius *R,* the circular fitting by Pratt method (Pratt 1987) was used to simulate a circle with estimation of the centre and radius based on the actual measurement fulfilled by Chernov (2021). The radius residuals were thence derived as the difference of the measurements and the estimated circle radius *R*, examining the planar precision from the GNSS measurement (Nickitopoulou et al. 2006).

To assess the precision on separate components, *E/N/U* residuals were computed. The reference model constructed for the *E/N* components were based on a sinusoidal model (Seibold 2021), in which the parameters are estimated by the discrete Fourier transform (DFT) and nonlinear fitting where frequency, amplitude, and phase of the most dominant peak of the DFT spectrum are used as initial values for the regression analysis (Psimoulis et al. 2015). For the Up component, since there were no movements in the vertical direction, it was assumed as stable during the test. Hence, the mean average of Up solutions was chosen as reference for the computation of the residuals in Up-component.

Results and discussion

All measurements regarding different rotation amplitudes were analysed for GPS, GPS + Galileo, and GPS + GLONASS + Galileo constellations. In this section, we show several representative results regarding the rotation radius of ~ 20 cm for GPS + GLONASS + Galileo solutions. It should be mentioned that the inter-frequency bias (IFB) associated with GLONASS ambiguity resolution, due to using receivers of different manufacturers in the rover and base (Msaewe et al. 2017; Wanninger 2012), was accounted by configuring the hardware bias term (i.e. − 0.055) in the RTKLIB, as suggested by Everett (2018). The GNSS solutions for different rotation amplitudes (5–50 cm) and the three different GNSS constellations (GPS-only, GPS + Galileo, and GPS + GLONASS + Galileo) were analysed to evaluate the performance of the low-cost GNSS receivers.

In Fig. 2 the *E* and *N* coordinates of the GPS + GLONASS + Galileo u-blox solution for the 20-cm radius experiment and the fit of the circle are presented. Figure 3 shows the *E* and *N* components time series of the 20-cm radius experiment and the corresponding spectra for the whole oscillation duration. In the spectra, it is evident that dominant frequency of 0.362 Hz corresponds to the rotation frequency. However, there are less dominant frequencies occurring at multiples of the dominant frequency, which might be caused by harmonics induced by distorted magnetomotive forces due to imperfectly sinusoidal-distributed winding slots in the rotation machine (Wakileh 2003; Psimoulis and Stiros 2008; Hohensinn et al. 2020). Based on the circular model fitting and the GNSS N/E time series, the radius of the circle was estimated, and the radius *N/E* residual time

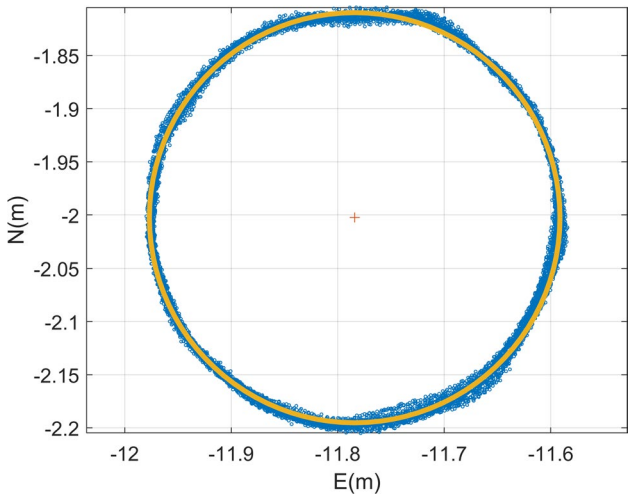

Fig. 2 The scatter plot of Northings versus Eastings for GPS + GLONASS + Galileo solutions of u-blox1 receiver and patch antenna as rover and Leica receiver and AS10 antenna as base with ~ 20 cm rotation radius, and the fitted circle based on Pratt method (orange) with the corresponding centre

series were derived. In Figs. 4 and 5, the residual time series of the radius and *N*/*E* components are presented, respectively. Based on the u-blox GPS + GLONASS + Galileo solution, the standard deviations of the *R*, *N*, and *E* residuals during rotation period are approximately 2.5 mm, 3.2 mm, and 2.3 mm, whereas for GPS + Galileo solution, the corresponding values are 3.5 mm, 3.9 mm, and 3.2 mm. The error ranges are about ± 1.0 cm for both *R* residuals and *N*/*E* components residuals. It is also noted from both spectra in Figs. 4 and 5 that the periodic pattern with frequency corresponding to the rotation frequency could be identified even in the residuals of *R* and *E*/*N*.

To demonstrate the multi-GNSS impact on the results, the precision of GPS-only, GPS + Galileo, and GPS + GLONASS + Galileo solutions were analysed from *R*, *E*/*N*/*U* residuals, respectively, and expressed in terms of standard deviation as shown in Table 1. It is observed that the relatively low precision of GPS-only solution of u-blox receiver, reaching 8.1 mm for the radius residuals, is enhanced significantly with the contribution of additional satellite systems, reaching 4.4 mm and 3.3 mm for GPS + Galileo and GPS + GLONASS + Galileo solutions, respectively. The beneficial contribution of the additional satellite systems is also observed in Leica GNSS solutions, which, however, is not that significant as for the low-cost GNSS receivers. For instance, the standard deviation of the *R* residuals was reduced from 5.2 mm for the GPS-only solution to 2.4 mm for the GPS + GLONASS + Galileo.

The analysis of the three GNSS solutions were applied for all the rotation radii, and it was confirmed the enhancement of the precision of the low-cost GNSS solution with the contribution of additional GNSS systems, reaching the highest precision for the GPS + GLONASS + Galileo solution. Figure 6 presents the precision of the GNSS solutions for *R*/*E*/*N*/*U* component for all the experiments. The precision enhancement is significant especially when Galileo is added in GPS-only solution. Also, the precision is the highest in *E* component due to the geometric restriction of the DD solution since the baseline direction is constrained to EW orientation (Habboub et al. 2020). Finally, the *U* component has the lower precision (i.e. highest standard deviation) due to the susceptibility of the patch antenna of the low-cost GNSS receivers to error sources such as multipath (Xue et al. 2021).

Low-cost GNSS receivers coupling

To investigate the consistency between the two closely coupled low-cost GNSS receivers for the low-frequency component and consequently model their potential common low-frequency biases due to error sources such as multipath, the *E*/*N*/*U* component of the low-cost GNSS time series were filtered. A low-pass Chebyshev filter of 0.1-Hz cut-off frequency was applied in *E*/*N*/*U* GNSS time series, which is a common approach applied in previous GNSS studies of similar applications (Msaewe et al. 2021). Then, the derived low-frequency component GNSS time series of the two low-cost GNSS receivers were analysed using cross-correlation.

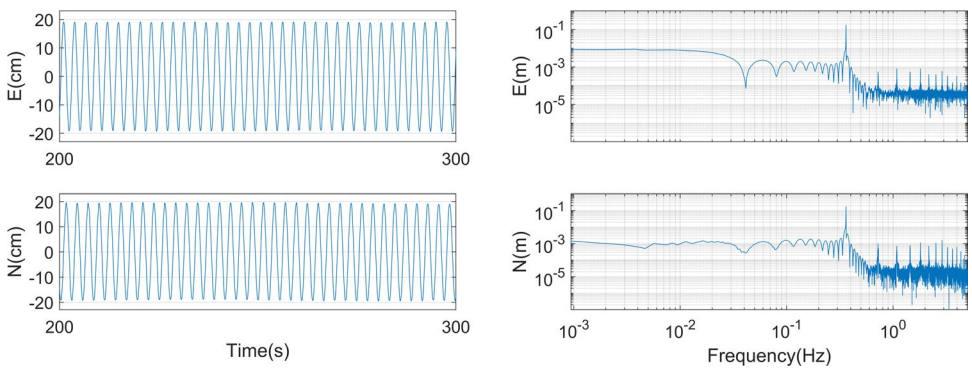

Fig. 3 Left: *E*/*N* GPS + GLONASS + Galileo time series expressing oscillatory motion around zero value after shifting the centre of the fitted circle to origin for a sample of 100 s; Right: DFT spectra of *E*/*N* components for the whole period during rotation

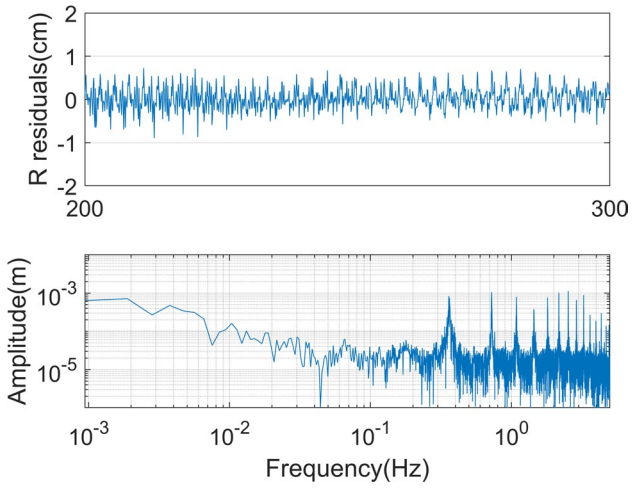

Fig. 4 (Top) *R* residual time series for GPS + GLONASS + Galileo solution of ~ 20 cm rotation radius test when u-blox1 and patch antenna are adopted as rover, Leica receiver and AS10 antenna as base. (Bottom) DFT spectral analysis for the *R* residual time series during rotation period

Figure 7 shows the low-frequency component of the *E*/*N*/*U* time series of the two low-cost GNSS receivers, revealing the similarity between the low-frequency component of the two low-cost GNSS receivers. The correlation coefficient between the two low-cost GNSS *E*/*N*/*U* low-frequency component time series were also summarised for GPS-only and multi-GNSS solution (Table 2). The low-frequency component of the low-cost GNSS receivers time series is strongly correlated, since the correlation coefficient is larger than 0.8, indicating a common pattern of low-frequency error in the two low-cost GNSS receivers. Thus, the application of the CME filter (Xue et al. 2021) partly mitigated the common low-frequency errors of the two low-cost GNSS receivers from the *E*/*N*/*U* time series, and the corresponding residual *E*/*N* time series was derived with higher precision. Table 3 presents the precision (standard deviation) of u-blox receiver after CME filtering, which is of similar level of that achieved after the high-pass filter in each u-blox receiver independently. The CME filtering is probably not that effective for the *U* component because of the weaker correlation between the two low-cost GNSS receivers in *U* component as indicated from the lower correlation coefficient.

Experiment of vertical motion

Experiment design

To assess the performance of the low-cost GNSS receivers in vertical dynamic motion, an experiment took place on the roof of NGI, by applying the experimental layout adopted in the study of Peppa et al. (2018). Figure 8 shows the heavy-duty tripod with the height-adjustable platform on top, where vertical motion of oscillation-type can be

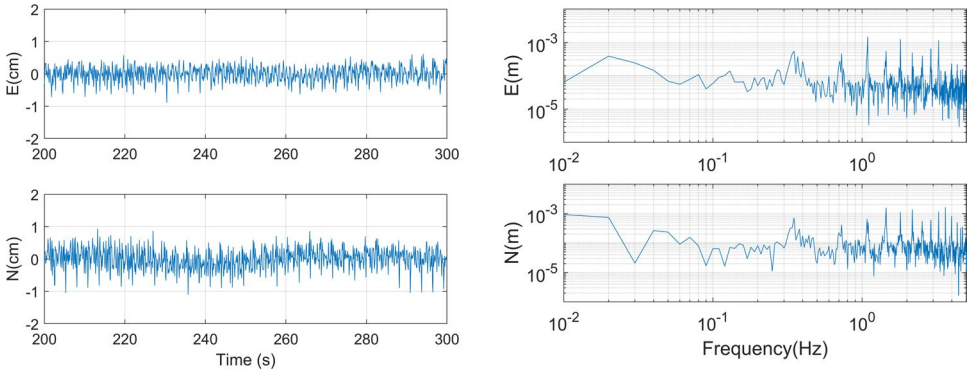

Fig. 5 (Left) *E*/*N* residual time series for GPS + GLONASS + Galileo solutions with u-blox1 receiver and patch antenna as rover and Leica receiver and AS10 antenna as base for ~ 20 cm rotation radius. (Right) Corresponding DFT spectra of *E*/*N* residuals

Table 1 Precision of radius (*R*) and *E*/*N*/*U* components for GPS-only (*G*), GPS + Galileo (*G* + *E*), and GPS + GLONASS + Galileo (*G* + *R* + *E*) measurement for u-blox and Leica rover with respect to rotation amplitude of ~ 20 cm for a period with 600-s duration during rotation; the precision of *U* is computed after applying the high-pass filter

Precision (mm)	u-blox			Leica		
	G	G + E	G + R + E	G	G + E	G + R + E
R	8.1	4.4	3.3	5.2	2.8	2.4
E	5.4	3.2	2.5	3.1	1.7	1.5
N	7.3	4.4	3.6	4.4	2.7	2.3
U	9.3	6.5	6.2	4.3	2.4	2.2

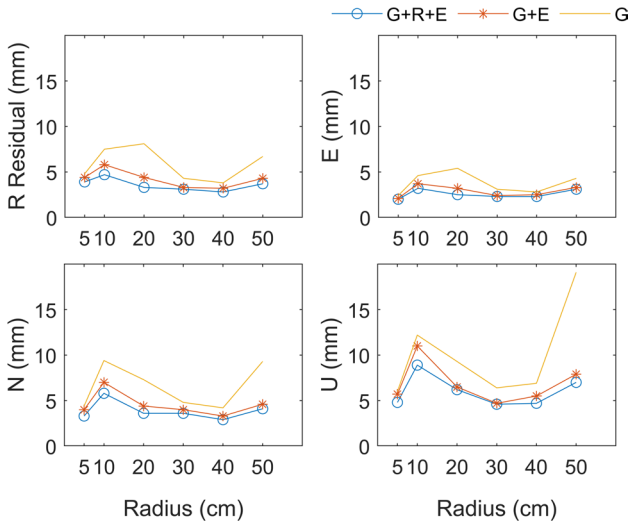

Fig. 6 The radius, *E*, *N*, and *U* precision bar chart for 5 to 50 cm rotation radii multi-GNSS solutions (GPS-only (*G*), GPS + Galileo (*G* + *E*), and GPS + GLONASS + Galileo (*G* + *R* + *E*))

executed manually. At the top of the adjustable platform, a Leica 360° prism is installed with a patch antenna attached to it via a metal plate. The metal plate was used to mitigate the multipath effect on the patch antenna and fix the position of the antenna firmly on the top of 360° prism. The tripod was levelled to ensure the verticality of the oscillation. The patch antenna was connected to a u-blox M8T receiver to monitor the vertical motion. A base station consisting of a Leica GR10 receiver and Leica AR25 antenna was installed about 10 m away to form a short baseline.

The GNSS receivers were configured to track and record GPS + GLONASS + Galileo signal at a sampling rate of 1 Hz. The Robotic Total Station (RTS) Leica TS30 was also set up on a control point on the roof at a distance of ~ 10 m, tracking and measuring prism motion at 10-Hz sampling rate. However, due to delays on distance measuring, the sampling-rate was not constant ranging between 4 and 7 Hz (Stiros et al. 2008). Since the patch antenna and the prism were appended to a rigid system, they both

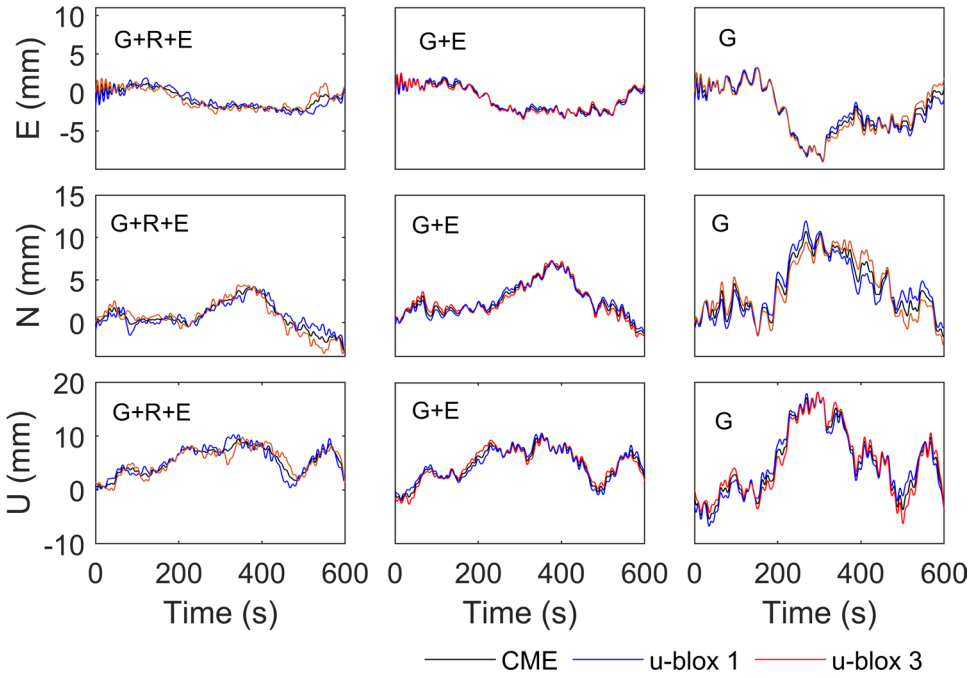

Fig. 7 Low-frequency component time series during the 20 cm rotation test oscillation period for u-blox1, u-blox3, and the CME low-frequency common mode error (CME), for GPS + GLONASS + Galileo (G + R + E), GPS + Galileo (G + E), and GPS only solution (GPS only)

Table 2 Correlation coefficient between the low-frequency components of the close spaced station time series for 5–50 cm radius rotation for GPS-only, GPS + Galileo, and GPS + GLONASS + Galileo constellation

R (cm)	GPS only			GPS + Galileo			GPS + GLONASS + Galileo		
	E	N	U	E	N	U	E	N	U
5	0.9	1.0	0.8	1.0	1.0	0.8	0.9	0.9	0.6
10	0.9	0.7	0.3	1.0	1.0	0.5	0.8	1.0	0.5
20	1.0	0.9	1.0	1.0	1.0	0.9	0.9	0.9	0.9
30	0.9	0.9	0.9	0.8	1.0	0.9	0.8	0.8	0.9
40	0.9	0.9	0.9	0.9	0.8	0.9	0.8	0.7	0.9
50	1.0	0.9	0.9	1.0	1.0	1.0	0.9	0.7	0.7

Table 3 Precision of radius (R) and $E/N/U$ components for GPS-only (G), GPS + Galileo ($G+E$), and GPS + GLONASS + Galileo ($G+R+E$) measurement for u-blox after the application of CME filtering and Leica rover with respect to rotation amplitude of ~ 20 cm for a period with 600-s duration during rotation; the precision of U is computed after applying the high-pass filter

Precision (mm)	u-blox 1		
	G	G+E	G+R+E
R	7.6	4.3	3.3
E	5.4	3.2	2.4
N	7.3	4.4	3.6
U	10.9	7.5	6.9

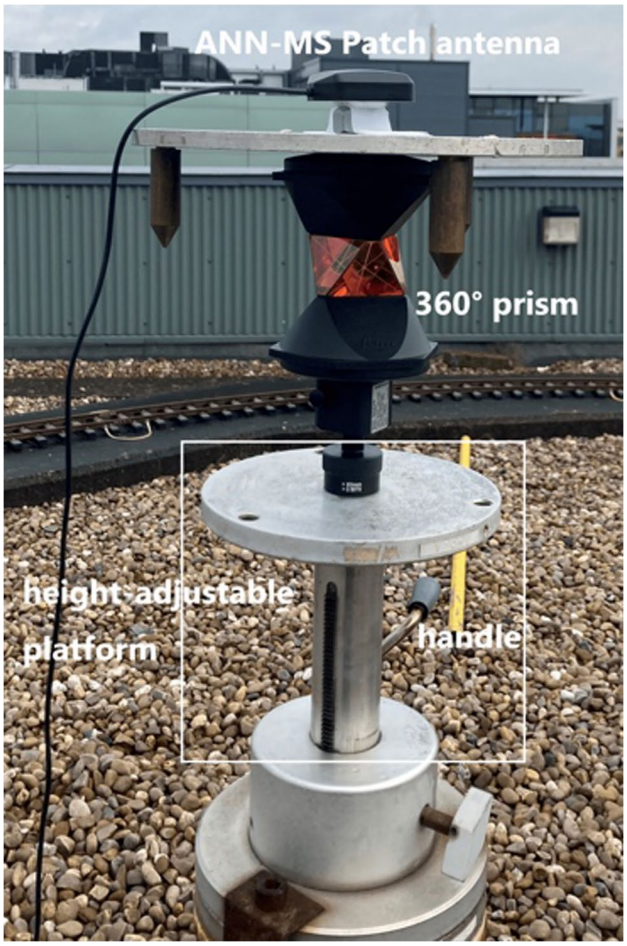

Fig. 8 The rover configuration of the vertical oscillation test

executed the same motion and the RTS measurements were used as the referencing truth for monitoring the vertical oscillation thanks to its high mm level of accuracy (Psimoulis and Stiros 2008). Hence, by comparing the low-cost GNSS with the RTS (TS30) results, the accuracy of the low-cost GNSS could be assessed.

The vertical oscillatory motion of the platform was achieved by rotating the handle manually in a uniform pace by referring to a metronome. Two experiments of vertical motion were executed of different amplitude and frequency: (i) a vertical motion of 0.2 Hz and ~ 8 mm amplitude and (ii) a vertical motion of 0.1 Hz and amplitude ~ 15 mm.

GNSS and RTS data analysis

The GNSS data were processed using the double difference method and the same version of RTKLIB open-source software as for GNSS data processing of the horizontal motion experiments. The same configuration and settings were applied which resulted to the baseline E/N/U GNSS time series as output. The RTS data were analysed and transformed in a local Cartesian coordinate system, resulting to $E/N/U$ time series of the prism positioning, with respect the position of the RTS (Psimoulis and Stiros 2007).

In the data analysis, the $E/N/U$ GNSS time series results were compared against the $E/N/U$ RTS time series, which was considered as the truth. In this case, the analysis was focused on the U component time series, which corresponded to the vertical motion, whereas the E/N component time series expressed only noise. Due to the unstable sampling rate of the RTS time series (Stiros et al. 2008), RTS data were initially linearly interpolated based on GNSS time to achieve synchronisation of the RTS and GNSS time series.

Results and discussion

The GPS-only solution of the low-cost GNSS receiver suffered from frequent false fixes, creating cycle slips which was resolved only by the contribution of additional satellite systems (Fig. 9). Thus, in this study, it was analysed only the GPS + Galileo and GPS + GLONASS + Galileo solutions of the low-cost GNSS receiver.

Figure 10 shows the Up-component of the GPS + Galileo, GPS + GLONASS + Galileo, and RTS time series of the two vertical motion tests. It is evident that in both tests, the excitation frequency can be detected equally accurately (i.e. 0.200 and 0.101 Hz) from both multi-GNSS solutions as from RTS time series. However, both multi-GNSS spectra are characterised by higher noise level, represented as (i) low-frequency coloured noise for frequency less than 0.1 Hz due to error sources such as multipath effect (Xue et al. 2021) and (ii) white noise for frequencies larger than 0.4 Hz, due to the higher noise level/random errors of the u-blox GNSS measurements.

To remove the low-frequency component of the GNSS time series, which expressed GNSS measurement noise, a Chebyshev type I high-pass filter of 8th order with cut-off frequency of 0.05 Hz was applied. The passband cutoff frequency of 0.05 Hz effectively extenuate the

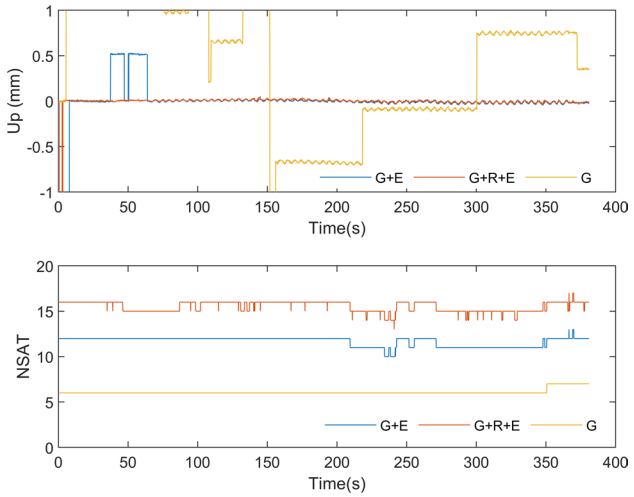

Fig. 9 GPS-only (G), GPS + Galileo ($G+E$), GPS + GLONASS + Galileo ($G+R+E$) time series for 8-mm vertical oscillation test and number of satellite (NSAT). The GPS-only solution, with NSAT around 6, suffers from frequent cycle slips

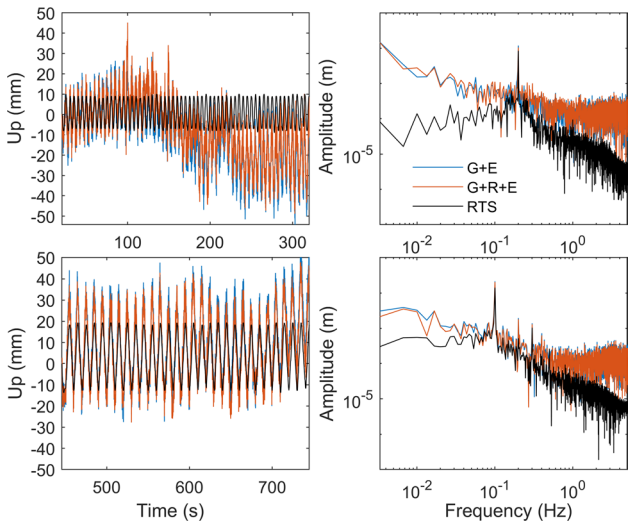

Fig. 10 Top panel: (left) the original u-blox $G+R+E$ and RTS Up time series and (right) corresponding DFT spectra; bottom panel: (left) the high-pass filtered u-blox and RTS time series and (right) corresponding DFT spectra, for the 8 mm, 0.2-Hz vertical oscillation test

multipath while still included the signal of the oscillatory motion. From the spectra of the high-pass filtered GNSS time series, it is evident that (i) the dominant frequency is detected as accurately as in the initial time series, (ii) the low-frequency error has been removed reaching the level of RTS time series, and (iii) the high-frequency (i.e. > 0.4 Hz) noise remains in the GNSS spectra.

Regarding the vertical motion amplitude, it is evident from Figs. 10 to 11 that the RTS time series could track the vertical motion to a high accuracy of mm level, indicating the oscillation amplitude of ~ 8 mm and ~ 15–16 mm, respectively. On the other hand, the oscillation amplitude derived from the high-pass filtered low-cost GPS + GLONASS + Galileo time series ranged between ~ 9 and ~ 20 mm for the 8-mm oscillation test and between ~ 20 and 30 mm for the 15-mm oscillation test. Based on these time series, the root mean squares (RMS) of u-blox and RTS were calculated, from which the amplitude of u-blox and RTS time series were estimated by multiplying the RMS with square root of 2 assuming a sinusoidal wave. From Table 4, it is shown that the RTS could accurately determine the amplitude of oscillation with mm-level accuracy. Regarding the low-cost GNSS time series, it seems that the GPS + GLONASS + Galileo is the most accurate since the oscillation amplitude deviates about 4–5 mm from the true oscillation amplitude, while for the GPS + Galileo solution, the corresponding deviation is 5–6 mm.

Case study: monitoring Wilford Suspension Bridge using low-cost GNSS receivers

To assess the performance of the low-cost GNSS receivers in monitoring bridge response and estimate its characteristics (response amplitude and modal frequency), the Wilford Suspension Bridge was used as the case study. The Wilford Suspension Bridge has been used as testbed in several previous studies of GPS/GNSS bridge monitoring applications, and its main characteristics are well-defined (i.e. main

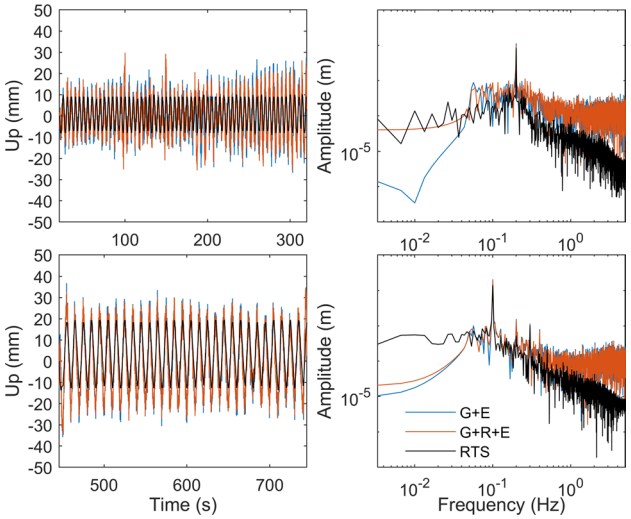

Fig. 11 Top panel: (left) the original u-blox $G+R+E$ and RTS Up time series and (right) corresponding DFT spectra; bottom panel: (left) the high-pass filtered u-blox and RTS time series and (right) corresponding DFT spectra, for the 15 mm, 0.1-Hz vertical oscillation test

Table 4 The RMS computed for u-blox and RTS time series in 8-mm and 15-mm vertical displacement and the estimated amplitude from RMS by multiplying the square root of 2 assuming sinusoidal waveform (unit: mm)

	u-blox (GPS + GLONASS + Galileo)		u-blox (GPS + Galileo)		RTS	
	RMS	Amplitude	RMS	Amplitude	RMS	Amplitude
8 mm	8.8	12.4	9.5	13.4	6.0	8.5
15 mm	14.4	20.3	15.1	21.3	10.2	14.4

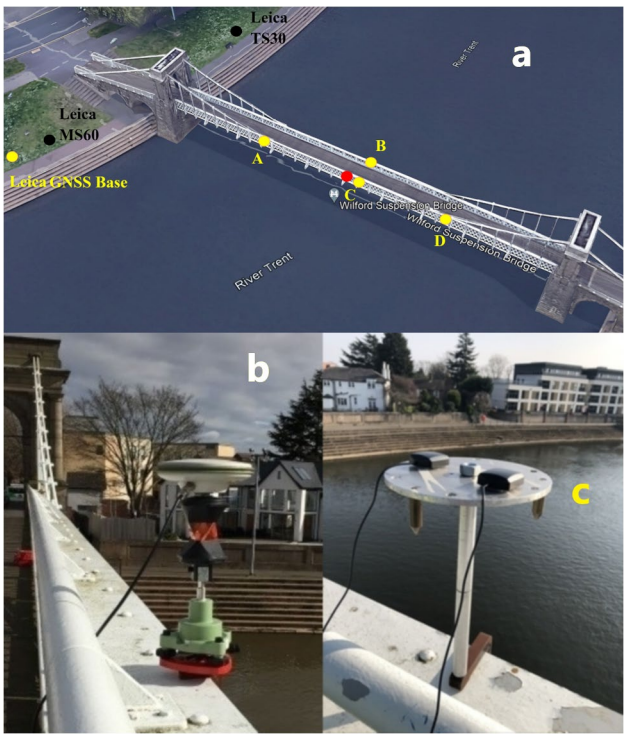

Fig. 12 **a** Location of the equipment and sensors along the riverbank and bridge (Leica TS30 and Leica MS60 are RTS); **b** the AS10 antenna at the midspan of the bridge with a 360° prism underneath; **c** deployment of the closely spaced low-cost patch antenna at midspan location C (red point)

modal frequency ~ 1.64 Hz, Psimoulis et al. 2016; Peppa et al. 2018). Therefore, it would be sufficient to evaluate the feasibility of the low-cost GNSS receivers in monitoring high-frequency (> 1 Hz) dynamic displacement of bridges.

Figure 12a presented the Wilford pedestrian suspension with the sensors location which were deployed along the bridge. In this study we focused at the sensors of point C, where the low-cost GNSS receivers were deployed (Fig. 12c), with a dual-frequency Leica station (Leica GS10 with AS10 antenna) and a prism set up in ~ 1 m distance from the low-cost receivers (Fig. 12b). A GNSS reference station (Leica GS10 and AS10) and a Robotic Total Station were set up on stable ground along the west riverbank of River Trent, free from excitations. RTS TS30 was tracking and recording the prism coordinates with 10-Hz sampling rate. However, due to unstable sampling rate of RTS, the actual acquisition frequency was in the range of 5–7 Hz as aforementioned (Stiros et al. 2008). RTS was recording in a pre-defined Cartesian coordinate system, with *x*-axis parallel to bridge longitudinal axis and *y*-axis parallel to bridge lateral axis. The GNSS receivers, geodetic and low-cost, were recording with 10-Hz sampling. The GNSS base station did not record Galileo satellites, and therefore, GPS-only and GPS + GLONASS solutions were feasible. The GNSS data were processed using the version of RTKLIB that was used in the experiments, producing the baseline results in *E*/*N*/*U* coordinates of the local coordinate system, which then was transformed to the bridge coordinate system aligned to the RTS coordinate system. The excitation of the bridge was generated by imposing the load by a cohort of people with different loading patterns and activities, such as walking, jumping, swinging, and marching.

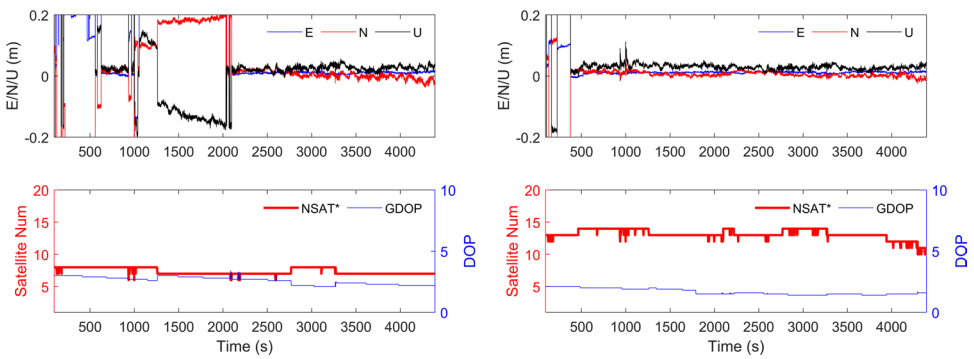

Fig. 13 (Left) GPS-only and (right) GPS+GLONASS *E*/*N*/*U* time series, the corresponding number of satellite (NSAT) and GDOP time series for the whole measurement period for u-blox1 at the Wilford Suspension Bridge

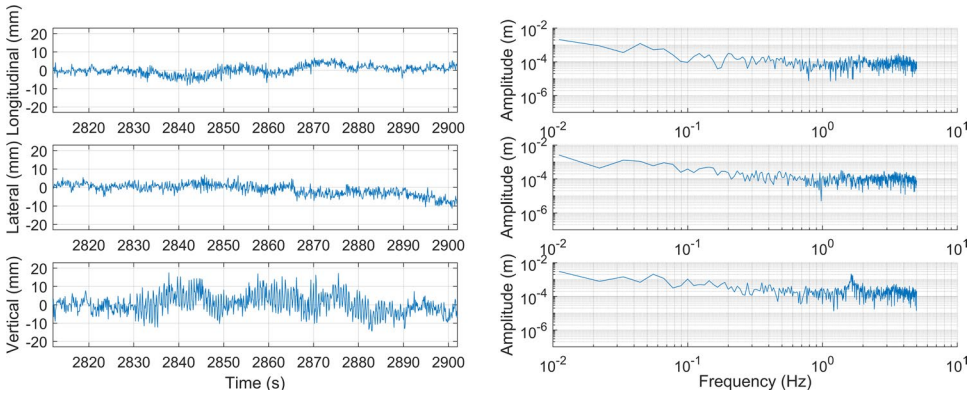

Fig. 14 (Left) u-blox1 Lon/Lat/Vertical original time series for excitation 05 and (right) the corresponding DFT spectra

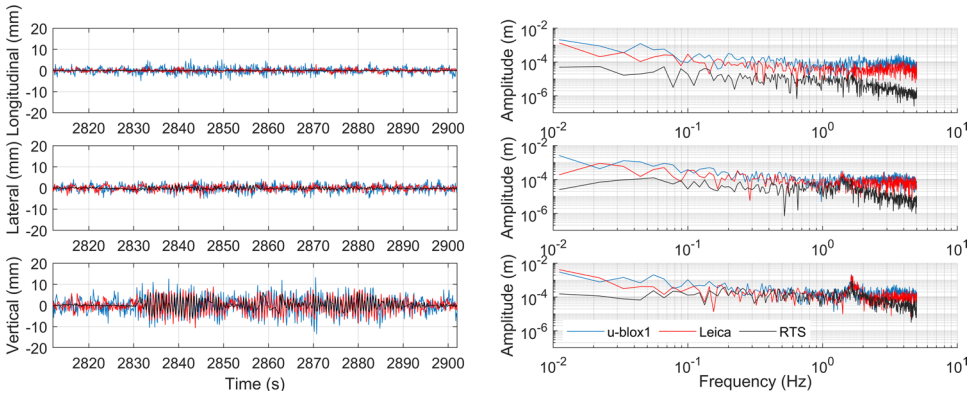

Fig. 15 (Left) U-blox1, Leica, and RTS high-pass filtered *Lon/Lat/Ver* time series for excitation 05 and (right) the corresponding time series DFT spectra

Figure 13A and B show the respective GPS-only and GPS + GLONASS *E/N/U* time series along with the corresponding satellite numbers and GDOPs during the monitoring period. It can be observed that the large offset-type deviations of the GPS-only solution is the result of cycle slips, occurred as a combination of the low number of satellites and poor quality of one or more GPS satellites signals. This cycle slips of the GPS solution was resolved by adding GLONASS satellite system and applying GPS + GLONASS solution. The latter was also observed in the geodetic-receiver solution confirming the results of previous studies (Msaewe et al. 2021). Therefore, for the following time-series analysis, GPS + GLONASS solutions were used

In the experiment, a total of 12 excitation activities with different loading pattern were carried out. In this case study, we present the analysis of the geodetic data (RTS, GNSS) for the excitation event 05, which corresponds to jumping activity at the mid-span of the bridge.

Figure 14 presents the original time series of the three components (i.e. longitudinal, lateral, and vertical) and the corresponding spectra for excitation 05. The spectrum of the vertical component revealed the main modal frequency of 1.680 Hz, even though the spectra of the lateral and vertical component were characterised by low-frequency noise.

To mitigate the low-frequency noise, we extracted the bridge dynamic response by applying a high-pass filter. The derived time series of u-blox1, Leica, and RTS measurements and the corresponding spectra are presented in Fig. 15. From the spectra of the vertical component, it was observed more clearly the main modal frequency for all three instruments (u-blox, Leica, RTS). In general, the GNSS spectra are noisier than the RTS as it was expected, whereas the u-blox seemed to be slightly noisier than Leica receiver, especially in the high-frequencies, characterised by larger white noise. However, the estimation of the modal frequency was clear and reliable with the u-blox measurements as with the other two techniques. Table 5 illustrates several parameters derived from excitation 05: (i) the modal frequency, which was detected from the spectral analysis; (ii)

Table 5 Frequency (Freq), amplitude (Amp), and noise level (represented by 1-sigma for 20 s before excitation period) in vertical component for excitation 05 using different measurement approaches

	RTS	Leica	u-blox1	u-blox2
Frequency (Hz)	1.676	1.676	1.676	1.676
Amplitude (mm)	3.6	4.5	4.5	5.5
Noise level (mm)	0.2	1.8	2.7	2.6

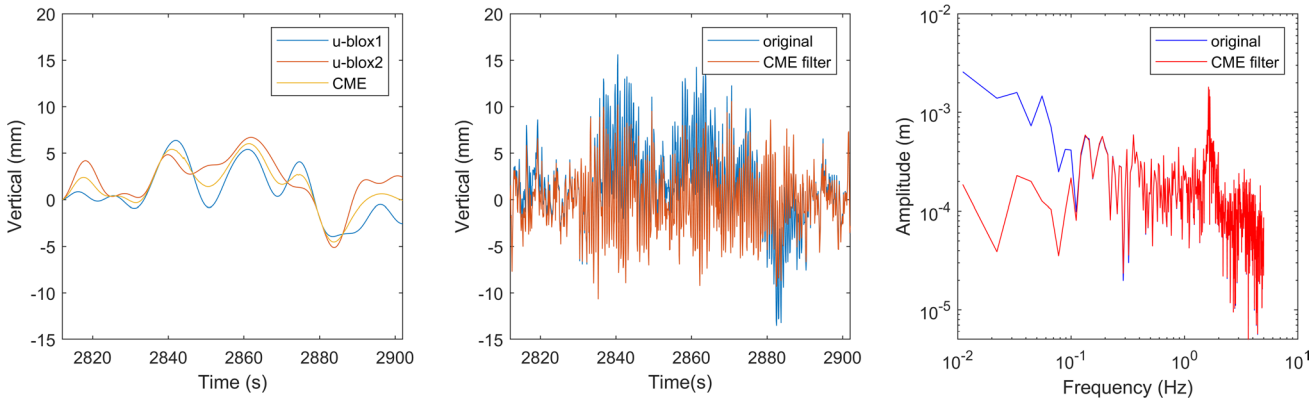

Fig. 16 (Left) u-blox1, u-blox2 low-pass filtered vertical time series, and simulated low frequency noise model based on CME for excitation 05. (Middle) weighted average combined original time series before and after CME filtering. (Right) spectra of weighted average original time series before and after CME filtering

the noise level, as the standard deviation of the period before the excitation; and (iii) amplitude estimation, corresponding to the maximum value of the standard deviation calculated adopting a 5-s moving window during the excitation period.

Based on the analysis of the two closely spaced low-cost GNSS receivers experiments, a high correlation (i.e. ~ 0.8) was detected for the closely spaced station low-frequency component, indicating a potential for common mode error (CME) filtering application to mitigate the long period noise usually present in GNSS time series (such as multipath; Peppa et al. 2018; Msaewe et al. 2021). It could be seen from Fig. 16 that the correlation between the low-frequency errors of the two closely spaced stations and the application of the CME filter is proved efficient in mitigating the low-frequency error within the time series and spectrum. The CME filtered average combined results was also capable to reduce the noise level from 2.7 mm of the individual u-blox high-pass filtered result to a value of 2.3 mm. The amplitude identified by adopting CME filter were also consistent and comparable with the high-pass filtered results with a value ~ 5.3 mm as compared to 5.5 mm from u-blox2 from Table 4.

Summary

In this paper, the low-cost GNSS receivers were assessed for their performance in monitoring dynamic response of civil engineering structures, such as bridges. The u-blox receivers were assessed based on controlled experiments in horizontal and vertical motion and a real bridge monitoring application. From the controlled experiments it was proved that the low-cost receiver is less precise than the dual-frequency GNSS receiver when GPS-only solution is applied, but the gap in the precision of the two receivers is significantly reduced for the multi-GNSS solution. The precision difference is reduced to a few mm. Furthermore, the u-blox receivers proved to be accurate in the estimation of the motion frequency. In the real bridge application, it was confirmed the beneficial contribution of the multi-GNSS solution for the low-cost GNSS receiver, as it was proved accurate with deviation of a few mm in the estimation of the bridge amplitude response and reliable in the estimation of the modal frequency (1.680 Hz). Also, the benefit of using multi-constellation was also shown with the improvement of the ambiguity fix rate. Therefore, future works could be conducted to examine the application of using the low-cost GNSS monitoring for a longer span bridge and assess different multi-constellations impact on the monitoring accuracy. The latter is in accordance with the application of low-cost sensors (MEMS, cameras, etc.) for the deformation monitoring of structures (Charalambous et al. 2015).

Funding This study has been supported by the Royal Society grant in the framework of the project "Reliability of single frequency GNSS precise positioning for ultra-range bridge deformation monitoring" (RA45UE).

Data availability The data that support the findings of this study are available from the corresponding author upon reasonable request.

Declarations

Conflict of interest The authors declare no competing interests.

References

Biagi L, Grec FC, Negretti M (2016) Low-cost GNSS receivers for local monitoring: experimental simulation, and analysis of displacements. Sensors (Basel) 16(12). https://doi.org/10.3390/s16122140

Charalambous E, Psimoulis P et al (2015) Measuring sub-mm structure displacement using QDaedalus: a digital clip-on measuring system developed for Total Stations. Appl Geomatics 7(2):91–101. https://doi.org/10.1007/s12518-014-0150-z

Chernov N (2021) Circle Fit (Pratt method). MATLAB Central File Exchange. Retrieved November 11, 2021 from https://www.mathworks.com/matlabcentral/fileexchange/22643-circle-fit-pratt-method

Cina A, Piras M (2015) Performance of low-cost GNSS receiver for landslides monitoring: test and results. Geomat Nat Haz Risk 6(5–7):497–514

Everett T (2016) Documentation of differences between RTKLIB demo5 and RTKLIB 2.4.3. [Blog post]. From http://rtkexplorer.com/downloads/rtklib-code/documentation-of-differences-between-rtklib-demo5-and-rtklib-2-4-3/. Accessed 14 Nov 2022

Everett T (2018) Glonass ambiguity resolution with RTKLIB revisited [Blog post]. Retrieved from https://rtklibexplorer.wordpress.com/2018/06/14/glonass-ambiguity-resolution-with-rtklib-revisited/. Accessed 14 Nov 2022

Everett T (2020) Demo5 b33c Binaries. Retrieved from http://rtkexplorer.com/downloads/rtklib-code/. Accessed 14 Nov 2022

Habboub M, Psimoulis P, Bingley R, Rothacher M (2020) A multiple algorithm approach to the analysis of GNSS coordinate time series for detecting geohazards and anomalies. J Geophys Res:Solid Earth 125(2):e2019JB018104

Heunecke O, Glabsch J, Schuhbäck S (2011) Landslide monitoring using low cost GNSS equipment n experiences from two alpine testing sites. J Civil Eng Archit 5(8). Accessed 14 Nov 2022

Hohensinn R, Häberling S, Geiger A (2020) Dynamic displacements from high-rate GNSS: Error modeling and vibration detection. Measurement 157:107655

Jo H, Sim SH, Tatkowski A, Spencer BF Jr, Nelson ME (2013) Feasibility of displacement monitoring using low-cost GPS receivers. Struct Control Health Monit 20(9):1240–1254

Manzini N, Orcesi A, Thom C, Brossault MA, Botton S, Ortiz M, Dumoulin J (2022) Performance analysis of low-cost GNSS stations for structural health monitoring of civil engineering structures. Struct Infrastruct Eng 18(5):595–611

Matias B, Oliveira H, Almeida J, Dias A, Ferreira H, Martins A, Silva E (2015) High-accuracy low-cost RTK-GPS for an unmannned surface vehicle. In OCEANS 2015-Genova 1–4. IEEE. Accessed 14 Nov 2022

Meng X, Nguyen DT, Xie Y, Owen JS, Psimoulis P, Ince S, Chen Q, Ye J, Bhatia P (2018) Design and implementation of a new system for large bridge monitoring – GeoSHM. Sensors 18(3):775

Msaewe HA, Hancock CM, Psimoulis PA, Roberts GW, Bonenberg LK, de Ligt H (2017) Investigating multi-GNSS performance in the UK and China based on a zero-baseline measurement approach. Measurement 102:186–199

Msaewe HA, Psimoulis PA, Hancock CM, Roberts GW, Bonenberg L (2021) Monitoring the response of Severn Suspension Bridge in the United Kingdom using multi-GNSS measurements. Struct Control Health Monit 28(11):e2830. https://doi.org/10.1002/stc.2830

Nickitopoulou A, Protopsalti K, Stiros S (2006) Monitoring dynamic and quasi-static deformations of large flexible engineering structures with GPS: accuracy, limitations and promises. Eng Struct 28(10):1471–1482. https://doi.org/10.1016/j.engstruct.2006.02.001

Peppa I, Psimoulis P, Meng X (2018) Using the signal-to-noise ratio of GPS records to detect motion of structures. Struct Control Health Monit 25(2):e2080. https://doi.org/10.1002/stc.2080

Poluzzi L, Tavasci L, Corsini F, Barbarella M, Gandolfi S (2019) Low-cost GNSS sensors for monitoring applications. Appl Geomat 12(S1):35–44

Pratt V (1987) Direct least-squares fitting of algebraic surfaces. ACM SIGGRAPH Comput Graph 21(4):145–152

Psimoulis PA, Stiros SC (2007) Measurement of deflections and of oscillation frequencies of engineering structures using Robotic Theodolites (RTS). Eng Struct 29(12):3312–3324. https://doi.org/10.1016/j.engstruct.2007.09.006

Psimoulis P, Stiros S (2008) Experimental assessment of the accuracy of GPS and RTS for the determination of the parameters of oscillation of major structures. Comput-Aided Civil Infrastruct Eng 23(5):389–403

Psimoulis P, Houlié N, Meindl M, Rothacher M (2015) Consistency of PPP GPS and strong-motion records: case study of Mw9.0 Tohoku-Oki 2011 earthquake. Smart Struct Syst 16(2):347–366. https://doi.org/10.12989/sss.2015.16.2.347

Psimoulis P, Peppa I, Bonenberg L, Ince S, Meng X (2016) Combination of GPS and RTS measurements for the monitoring of semi-static and dynamic motion of pedestrian bridge. In Proc 3rd Joint Int Symp Deformation Monit-JISDM, Vienna, Austria, March 30 – April 2, 2016

Seibold P (2021) Sine fitting. MATLAB Central File Exchange. Retrieved November 11, 2021 from https://www.mathworks.com/matlabcentral/fileexchange/66793-sine-fitting

Stiros S, Psimoulis P, Kokkinou E (2008) Errors introduced by fluctuations in the sampling rate of automatically recording instruments: experimental and theoretical approach. J Surv Eng 134(3):89–93

Takasu T, Yasuda A (2008) Evaluation of RTK-GPS performance with low-cost single-frequency GPS receivers. In Proc Int Symp GPS/GNSS 852–861

Takasu T, Yasuda A (2009) Development of the low-cost RTK-GPS receiver with an open source program package RTKLIB. In Int Symp GPS/GNSS 1. International Convention Center Jeju Korea.

Wakileh GJ (2003) Harmonics in rotating machines. Electr Power Syst Res 66(1):31–37

Wanninger L (2012) Carrier-phase inter-frequency biases of GLONASS receivers. J Geodesy 86(2):139–148

Xue C, Psimoulis P, Meng X (2022) Feasibility analysis of the performance of low-cost GNSS receivers in monitoring dynamic motion. Measurement 202:111819

Xue C, Psimoulis P, Zhang Q, Meng X (2021) Analysis of the performance of closely spaced low-cost multi-GNSS receivers. Appl Geomatics 1–21.

Zhang L, Schwieger V (2016) Improving the quality of low-cost GPS receiver data for monitoring using spatial correlations. J Appl Geodesy 10(2):119–129